Journal of Ceramic Processing Research. Vol. 26, No. 2, pp. 209~218 (2025)
(Received 4 November 2024, Received in revised form 12 February 2025, Accepted 1 March 2025)
https://doi.org/10.36410/jcpr.2025.26.2.209

J O U R N A L O F
Ceramic Processing Research

Investigating the growth and corrosion resistance of Mg-Li alloy modified by in situ steam coating

Jumei Zhang*, Hui Gao, Duoduo Lian, Ning Luo, Jingwen Wu and Chaochao Wang
School of Materials Science and Engineering, Xi'an University of Science and Technology, Xi'an 710054, China

This paper investigates the effect of in-situ steam time on the growth and corrosion resistance of the steam coating (SC) on the surface of LA103Z Mg-Li alloy. The morphology and phase of the SC were studied by scanning electron microscopy (SEM), X-ray diffraction (XRD) and fourier transform infrared spectroscopy (FT-IR). The corrosion resistance of the coating was studied by hydrogen evolution and immersion test. In addition, the growth mechanism and corrosion resistance mechanism of steam coating were also analyzed. It was found that the density and thickness of the coating increased with the extension of in-situ steam time. However, excessive extension of the in-situ steam time will lead to the destruction of the porous and dense membrane structure. It can be seen from the results of the immersion experiment that the minimum hydrogen evolution per unit area of SC-6 h after eight days of immersion is only 8.71 mL/cm^2, which is much smaller than the base body (37.74 mL/cm^2).

Keywords: Mg-Li Alloy, LDH, In-situ steam coating, GRowth, COrrosion resistance.

Introduction

As China strives towards carbon neutrality and peaking, magnesium-lithium (Mg-Li) alloy, a lightweight alloy material, has emerged as a green engineering material for the 21st century, pivotal to sustainable industrial development [1].

Among the structural metal materials, Mg-Li alloy has the lowest density, high specific strength and specific stiffness, high thermal conductivity, can absorb impact energy, excellent performance of vibration and noise reduction, and remarkable shielding effect of electromagnetic interference. It will be widely applied in the fields of auto, 3C, pharmacy and aerospace [2-6]. Mg-Li alloy, however, is often highly reactive elements. Mg-Li alloy tend to corrode under water or other corrosives, which have a negative effect on their mechanical properties, leading to a thinning of the alloy itself and an increase in the amount of oxides, which may result in structural damage. The extensive application of magnesium alloy is seriously hindered. Two methods are commonly used to enhance the anti-corrosive properties of magnesium: alloying and surface modification [7, 8]. Nowadays, many researches have been done on the basis of surface modification, such as chemical transformation coating [9-11], microarc oxidation [12-14], chemical plating [15-17] and coating. In terms of coatings, layered double hydroxide have attracted the attention of many scholars because of their special layered structure, excellent controllable properties and remarkable corrosion resistance, and have become a research hotspot in the field of anti-corrosion coatings in recent years [18, 19].

LDH (Layered double hydroxide) is a composite hydroxide composed of divalent sum and metal substances. The ion group of the laminate is attached to the main layer through electrostatic attraction, hydrogen bond or subbond, so as to control the charge balance. The structure of LDH permits the insertion of a variety of molecules between layers, and because the layers are not interconnected, it is possible to increase the distance between them to obtain a single nanosheet [20]. It has the properties of flame retardant, ion-exchange, thermal, adsorption, catalytic and anti-corrosion [21-23]. The methods of preparing LDH on the surface of Mg-Li alloy include co-deposition [25], in-situ growth [26, 27], ion-exchange [28-30], electrodeposited [31-33] and plasma spray [34]. At present, the main preparation methods of LDH are hydrothermal method and coprecipitation method. However, these two preparation methods take a long reaction time, use toxic chemicals, the operation is complex and difficult to control, and produce many by-products. Under this research background, there is an urgent need for a simple and green method. Hydrothermal and steam coating [35] methods are commonly used for the preparation of LDH coatings on magnesium alloy. Compared to the liquid environment, the dissolution of Mg^{2+} and Al^{3+} in water will not occur. In the steam environment, the coating forming efficiency

*Corresponding author:
Tel : +86-29-85587373
Fax: +86-029-85583138
E-mail: feiyue-zjm@163.com

of this process is higher. In recent years, the steam coating method has gained widespread attention due to its excellent bonding capabilities. It is a non-chemical reaction process that can be used for the protection of Mg-Li alloy [36-38]. It is a new effective protective method for Mg-Li alloy.

In 2013, Ishizaki, as a newly developed technology for preparing LDH, has demonstrated that Mg $(OH)_2$/Mg-Al-LDH is highly corrosion-resistant on magnesium alloys [36]. Zhang et al. prepared Mg-Al layered double hydrogen oxidation/steam coating (LDH/SC) on LA43M Mg-Li alloy surface by steam treatment and in situ hydrothermal method. The effects of hydrothermal time on the growth characteristics, wear resistance and corrosion behavior of LDH/SC in 3.5 wt.% NaCl solution were systematically studied. The results showed that appropriate extension of hydrothermal reaction time was beneficial to the nucleation and growth of LDH. When the hydrothermal time is 30 h, the prepared coating density is the best, and the prepared coating can significantly improve the corrosion resistance and friction and wear properties of the substrate. Generally speaking, in the in-situ steam coating method, reaction temperature and reaction time, steam/liquid environment, steam pressure, solution PH value, etc. will affect the formation of LDH [39]. Under steam condition, Ishizakiet put AZ31 Mg alloy into the reactor. Orthogonal test was carried out at different reaction temperatures (423 K-453 K) and the number of times (1 h-8 h) [40]. Ke et al. investigated the formation of LDH by immersing Mg alloy directly in liquid water or exposing it to water steam. The results show that the protective coating produced by in-situ steam coating has unique surface morphology, and its corrosion resistance is obviously better than that of direct immersion [41]. Nakamura et al. investigated the influence of steam pressure change on the formation of corrosion-resistant LDH on AZ61 magnesium alloy by in-situ steam coating method. The results show that the thickness of the coating remains unchanged even when the steam pressure value changes. However, with the increase of steam pressure, the production of Mg-Al-LDH decreases, resulting in the expansion of Mg-Al-LDH interlayer spacing and the decrease of coating density. A large number of small cracks were observed in the coating layer, which made it prone to pitting. Therefore, the ratio of Mg-Al-LDH to $Mg(OH)_2$ can be increased by changing the vapor pressure in the reactor, thus improving the corrosion resistance of the LDH [42].

At present, the research system of preparing SC on the surface of magnesium-lithium alloys by in-situ steam coating method is not perfect, and it tends to carry out research on the LDH prepared by the in-situ steam method as well as the LDH composite coating. Zhang et al. showed that the composite coating has a significant enhancement on the corrosion resistance of magnesium alloy through the study of LDH/SC, but to form a good composite coating, the preparation of SC has a crucial role. Therefore, in this experiment, Mg-Al-LDH were prepared on the surface of LA103Z Mg-Li alloy for different times (3 h, 6 h, 9 h, 12 h) by in situ steam method. It is aimed to study the effects of different times on SC morphology, composition and corrosion resistance, and finally optimise the optimal time parameters suitable for SC growth on LA103Z substrate.

Experiment

Experimental materials

In this experiment, the weight percentages of each element of LA103Z Magnesium-lithium alloy were as follows: Li 9.5-10.5, Al 2.5-3.5, Zn 2.5-3.5, Si 0.5, Fe 0.05, Cu 0.05, other 0.3, equilibrium Mg) as the matrix. Before the experiment began, it was divided into thin pieces with dimensions of approximately 22 mm × 22 mm × 3 mm using wire cutting technology. Due to the active chemical properties of LA103Z ultra-light magnesium lithium alloy, it is easy to oxidize under natural conditions and form a certain thickness of oxide coating, so it is necessary to use 200 #, 400 #, 800 #, 1000 #, 2000 #, 3000 #, 5000 # sandpaper to polish the surface until smooth and flat before the experiment starts. Then the polished sample is placed in the ultrasonic cleaning machine and cleaned with anhydrous ethanol for 15 min to completely remove the oxide coating on its surface. After cleaning, the sample was taken out and rinsed and dried with deionized water.

Preparation of SC

The pre-treated LA103Z matrix and deionized water were added to the hydrothermal synthesis reactor, and the temperature of the constant temperature blast drying oven was set at 110 °C, with the time parameter varying from 3 h, 6 h, 9 h, 12 h, to prepare SC at different times. After in-situ steam treatment, the surface of the sample was cleaned with deionized water, and the prepared sample was labeled as SC-3 h, SC-6 h, SC-9 h and SC-12 h successively, and then dried and stored.

Characterization and testing

The scanning electron microscope (SEM, VEGA II XMU) produced by TESCAN of the Czech Republic was used to observe the surface morphology and cross section morphology of the coating layer samples, in which the surface was secondary electron imaging and the cross section was backscattered electron imaging. At the same time, the composition and elements of SC was detected and analyzed by EDS (OXFORD 7718) attached to SEM.

X-ray diffractometer (XRD, PANalytical) produced by Dutch company PANalytical was used to determine the phase composition of the coating layer. The diffractometer uses a continuous scanning mode, using the Cu target as the anode ($\lambda_{K\alpha}$=0.15416 nm), the tube voltage and tube current are 40 kV and 8 mA, respectively, the scanning

speed is 3.74°/min, the Angle range of diffraction is 10~80°, and the step size is 0.01°.

The Fourier transform infrared spectrometer (FTIR, Nicolet IS5) produced by Thermo Fisher Scientific was used to further analyze the structure of the coating samples. The test sample was powder, and the scanning range of the spectrometer was 4000~500 cm^{-1}.

An electrochemical workstation (PARSTAT4000) produced by Advanced Measurement Technology Co., Ltd. in the United States was used to detect the electrochemical corrosion properties of the coating samples. The electrolytic cell uses a three-electrode system, with saturated AgCl electrode as the reference electrode, platinum electrode as the opposite electrode, and coating sample as the working electrode. The 3.5 wt.% NaCl solution was used as the electrolyte, and the exposed area was 1 cm^2. Before the electrochemical impedance test and polarization test, the open-circuit potential measurement is performed for 30 min to ensure that the potential fluctuation is relatively stable. The disturbance potential of electrochemical reactance is 10 mV (RMS), and the scanning frequency range is 10 mHz~100 KHz. The scanning rate of the potentiodynamic polarization curve test is 4 $mV \cdot s^{-1}$.

In order to further investigate the long-term corrosion resistance of Mg-Li alloy, hydrogen evolution tests were carried out on matrix and coating samples. This method measured the corrosion resistance of the coating layer by calculating the hydrogen precipitation per unit area of the sample in 3.5 wt.% NaCl solution. The test time was set to 8 days, and the surface area of the sample was to be measured before the experiment. During the test, the sample should be put into the solution, and the funnel should be inverted on the sample. Record the initial reading of the titer and record it every 48 hours. Three independent hydrogen evolution experiments were performed for each parameter to ensure the reliability of the data.The formula for calculating hydrogen evolution per unit area is:

$$V = \Delta V/S \quad (1)$$

Where V is the cumulative amount of hydrogen precipitation per unit effective surface area, unit $mL \cdot cm^{-2}$, ΔV is the cumulative amount of hydrogen precipitation, unit mL, S is the relative surface area of the specimen. $S=2ac+2bc+1.5ab$, unit cm^2, where a, b and c are the length, width and thickness of the specimen, respectively.

Immersion testing was used, which involves immersing the SC specimens in 3.5 wt.% NaCl solution for 8 d. By analysing the SC morphology after immersion, the differences in corrosion morphology under different in situ steam treatment temperatures were explored, and finally the temperature parameters of SC with dense structure and better corrosion resistance were obtained.

Results

Steam coating characterization

Fig. 1 shows the surface morphologies of SC prepared on the surface of LA103Z magnesium alloy under different in situ steam treatment times. Fig. 1(a), (b) shows that when the in situ steam treatment time is 3 h, only a small amount of flake material is formed on the surface of the substrate. When the in situ steam treatment time is extended to 6 h, the size and quantity of the nano-sheets increase, and the surface of the magnesium alloy is basically covered completely. At this time, the nano-sheets grow perpendicular to the surface of the matrix. When the in situ steam treatment time is 9 h, the distribution of nanosheets is still uniform, but there are local phenomena such as collapse and stacking, which affect the density of the coating to a certain extent. When the time was extended to 12 h, in addition to the nanosheet structure, massive materials were formed on the surface of the matrix. It can be observed from Fig. 1(h) that the size and distribution of SC nanosheets prepared under this time parameter were different and uneven.

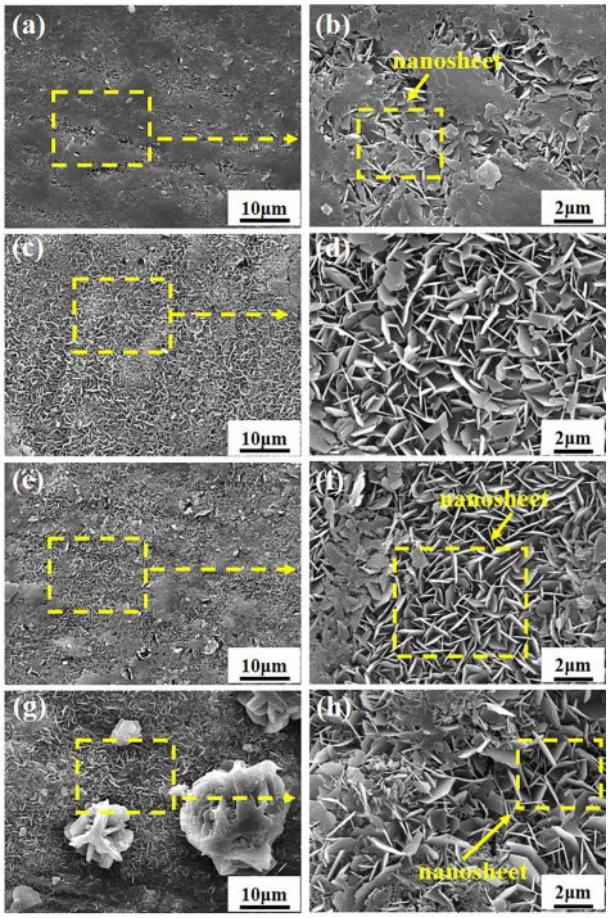

Fig. 1. Surface SEM images of SC prepared with different in situ steam treatment time: (a, b) SC-3 h; (c, d) SC-6 h; (e, f) SC-9 h; (g, h) SC-12 h.

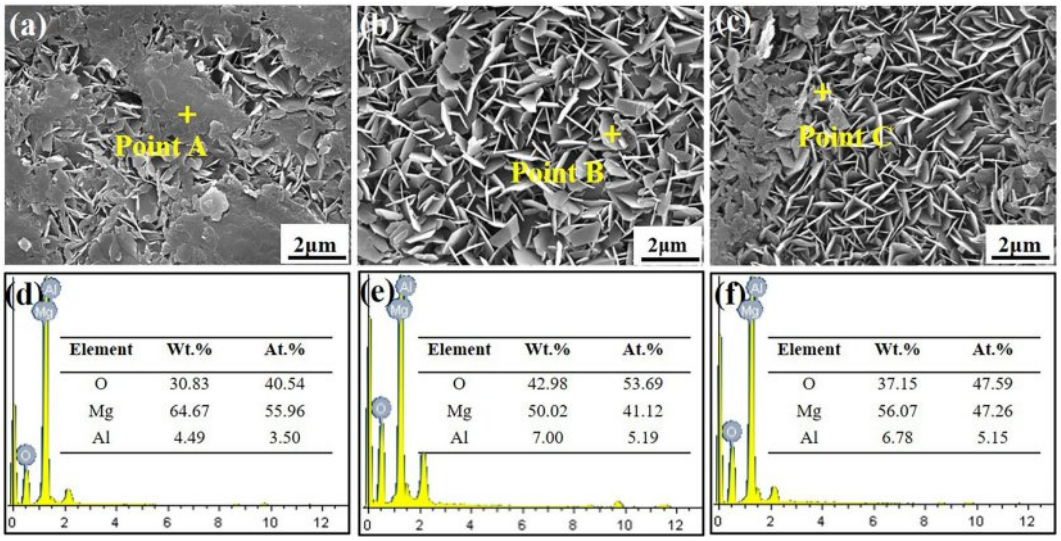

Fig. 2. EDS scanning results of SC surface: (a, d) SC-3 h; (b, e) SC-6 h; (c, f) SC-9 h.

Fig. 2 shows the point scanning results of SC-3 h, 6 h and 9 h samples. Compared with Fig. 2(d), (e), (f), it can be seen that the O element weight percentage and Al element weight percentage of the SC prepared at 6 h in situ steam treatment time are the highest, and the Mg element weight percentage of the SC-6 h is 50.02%, which is lower than the coating prepared at 3 h and 9 h. The Mg element is mainly derived from MgO and $Mg(OH)_2$ generated in the matrix and in situ steam treatment process. The presence of Al element indicates that the SC is not only composed of MgO and $Mg(OH)_2$.

Fig. 3 shows the cross section morphology of SC prepared on the surface of LA103Z magnesium alloy under different in situ steam treatment times. Fig. 3(a) shows that when the in situ steam treatment time is 3 h, the coating layer is tightly bound to the substrate, and the thickness of the coating layer is only 0.724 μm. When the in situ steam treatment time was extended to 6 h and 9 h respectively, the thickness of the coating increased to about 2.647 μm and 2.608 μm, and the coating was uniform and dense without obvious defects. However, when the in situ steam treatment time was extended to 12 h, obvious pores appeared in the coating layer (Fig. 3(d)), and the structure of the coating layer was damaged

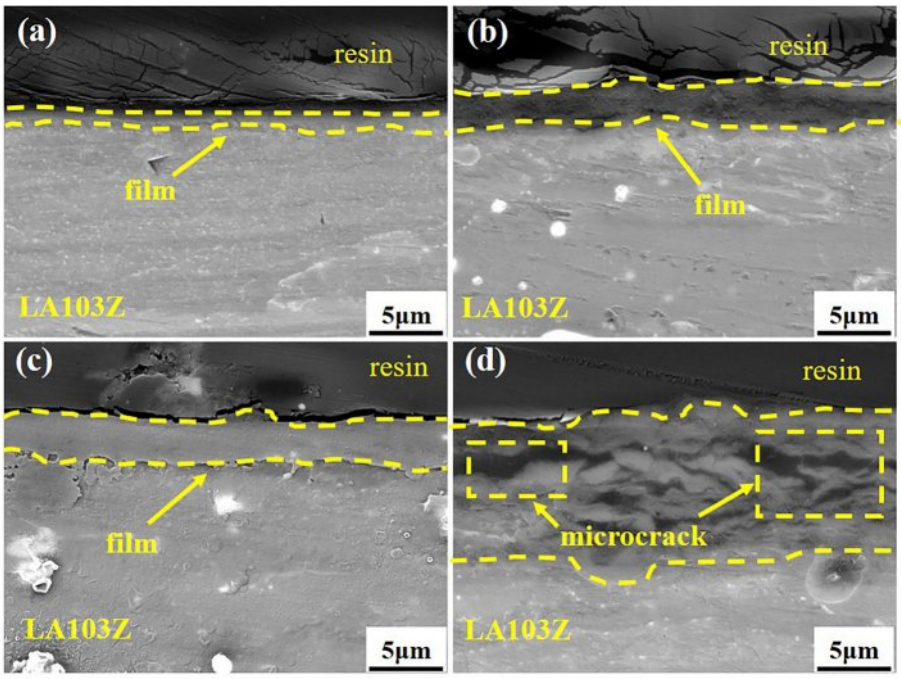

Fig. 3. Cross-section SEM images of SC prepared with different in situ steam treatment time: (a) SC-3 h; (b) SC-6 h; (c) SC-9 h; (d) SC-12 h.

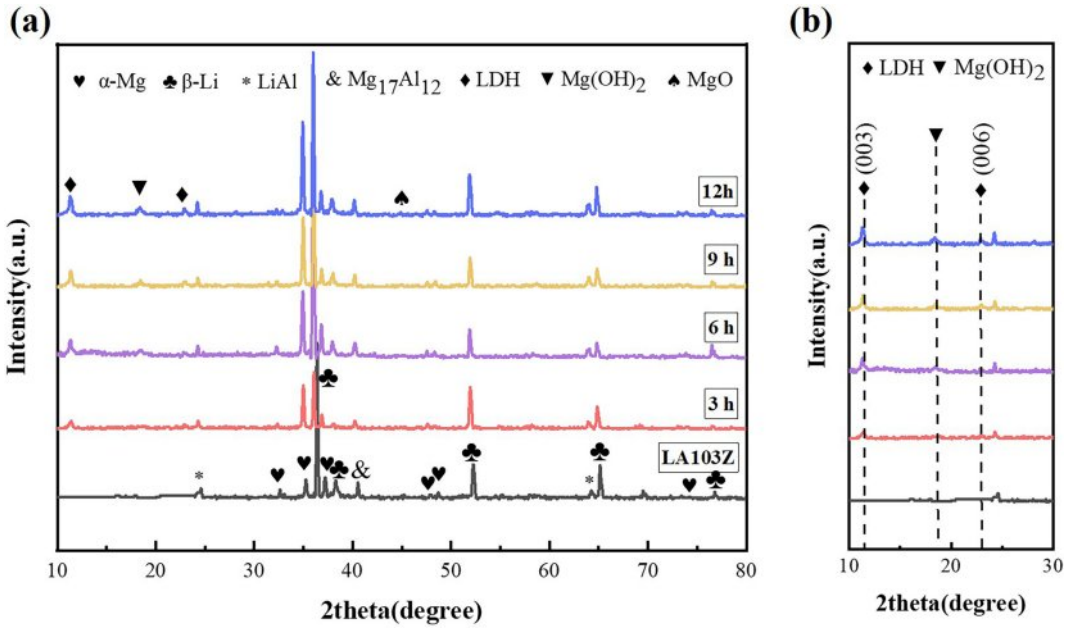

Fig. 4. XRD patterns of LA103Z and SC prepared with different in situ steam treatment time in the range of (a) 10°~80°; (b) 10°~30°.

and no longer dense. The thickness and structure of the coating can not be optimized by simply prolonging the in situ steam treatment time.

XRD and FI-IR analysis

Fig. 4 shows the X-ray diffraction patterns of SC samples prepared on the surface of LA103Z substrate and at different in situ steam treatment times. It can be seen from the figure that the phase composition of the matrix mainly includes α-Mg phase, β-Li phase, LiAl phase and $Mg_{17}Al_{12}$ phase. Compared with the matrix, the new phase appeared in the SC samples prepared under different in situ steam treatment time. The characteristic diffraction peaks of $Mg(OH)_2$ and MgO were found in the vicinity of 2θ=18.2° and 44.8°, respectively, indicating that the SC is mainly composed of $Mg(OH)_2$ and MgO phases. The (003) and (006) characteristic peaks of Mg-Al-LDH were detected at about 2θ=11.2° and 22.9°, respectively, that is, a small amount of LDH was also generated during in situ steam treatment.

Fig. 5 shows the Fourier transform infrared absorption spectra of SC prepared on the substrate surface under different in situ steam treatment times. The Mg-O absorption band appeared at 487 cm^{-1} in different coating layers, and the Mg-O-H bond stretching vibration peak appeared at 3696 cm^{-1}. The absorption bands at 3447 cm^{-1} and 1633 cm^{-1} were corresponding to the stretching vibration of -OH bond and the bending vibration of water molecules, respectively. The absorption peak at 2922 cm^{-1} is caused by the stretching vibration of the C-H bond. The presence of these absorption peaks confirmed that the main components of SC were $Mg(OH)_2$ and MgO.

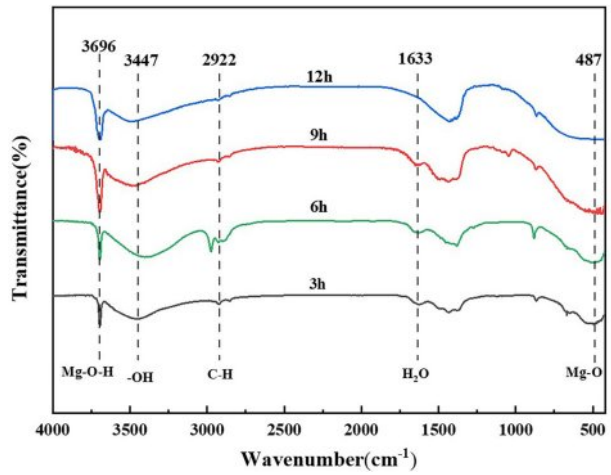

Fig. 5. FT-IR spectra of SC prepared with different in situ steam treatment time.

Corrosion resistance of steam coatings

Hydrogen evolution test was carried out on SC and matrix prepared on LA103Z surface under different in situ steam treatment time, and the results were shown in Fig. 6. The hydrogen evolution per unit area of each sample showed an increasing trend over time. The results show that the coating s prepared under different time parameters have protective effects on the matrix, and the protective effect of SC-6 h is the most obvious. After soaking for 192 h, the hydrogen evolution volume per unit area of the matrix reached the maximum, about 37.74 mL/cm^2, and the hydrogen evolution volume per unit area of SC-6 h was the minimum, about 8.71 mL/cm^2. At this time, the hydrogen evolution capacity per unit area of the SC prepared at 3 h, 9 h and 12 h

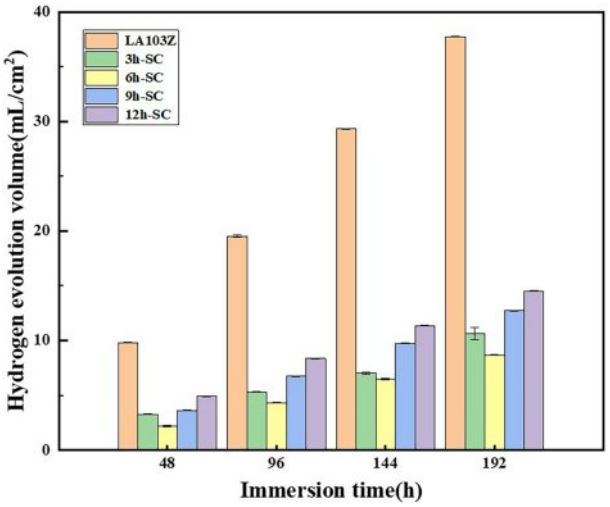

Fig. 6. Hydrogen evolution per unit area of LA103Z and SC prepared with different in situ steam treatment time immersed in corrosion solution for 192 h.

were 10.89 mL/cm^2, 12.74 mL/cm^2 and 14.52 mL/cm^2, respectively, and the corrosion resistance of the coatings first increased and then decreased with the extension of time. When the time parameter is 12 h, the defects of the coating layer make the corrosion solution easily penetrate the coating layer and corrode the matrix.

Corrosion morphology

Fig. 7 shows the morphology of SC prepared under different in situ steam treatment times before and after immersion in 3.5 wt.% NaCl solution for 192 h. From the macroscopic morphology, the surface structure of the coating prepared under different time parameters was complete, and the coating was corroded to a certain extent after immersion for eight days. Among them, SC-3 h and SC-12 h have the most serious corrosion, and the surface of the coating becomes no longer smooth after immersion, and white corrosion remains around the corrosion pit. This is because the thickness of the coating

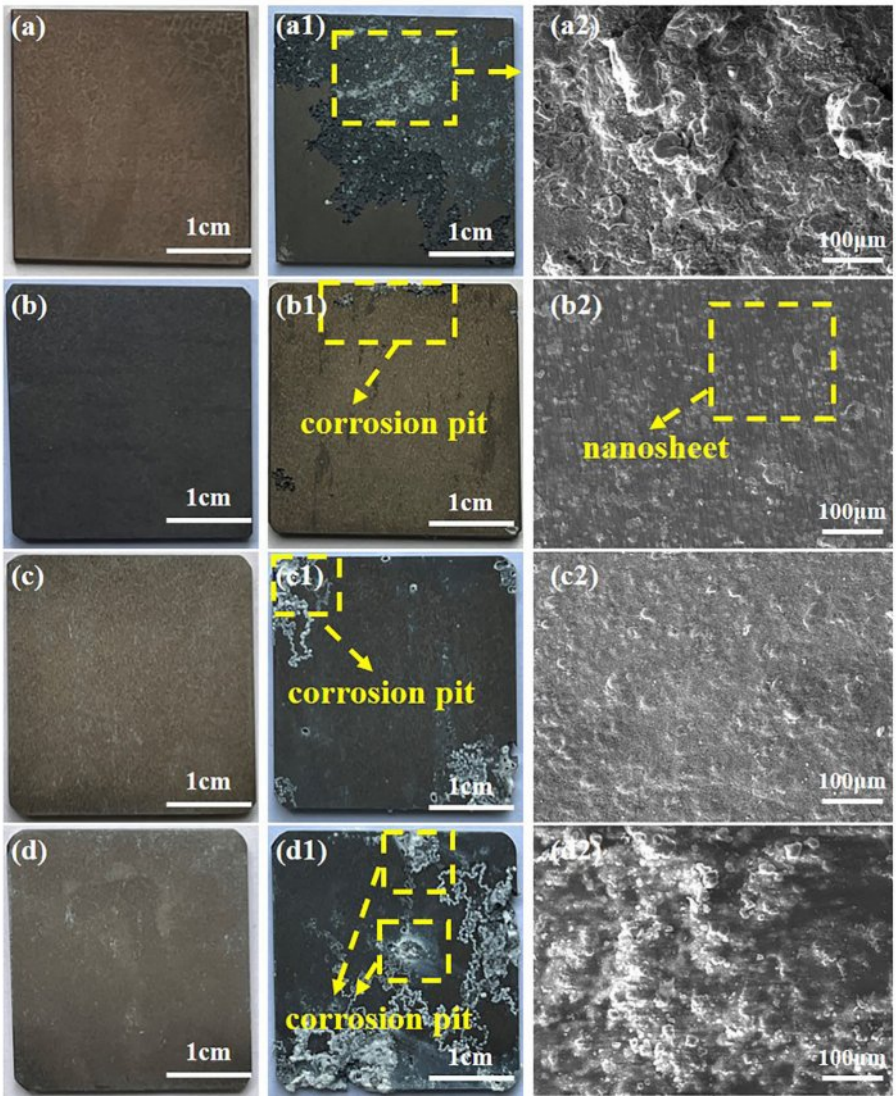

Fig. 7. Surface morphologies of SC prepared with different in situ steam treatment time before and after immersion in 3.5 wt.% NaCl solution for 192 h: (a, a1, a2) 3 h; (b, b1, b2) 6 h; (c, c1, c2) 9 h; (d, d1, d2) 12 h.

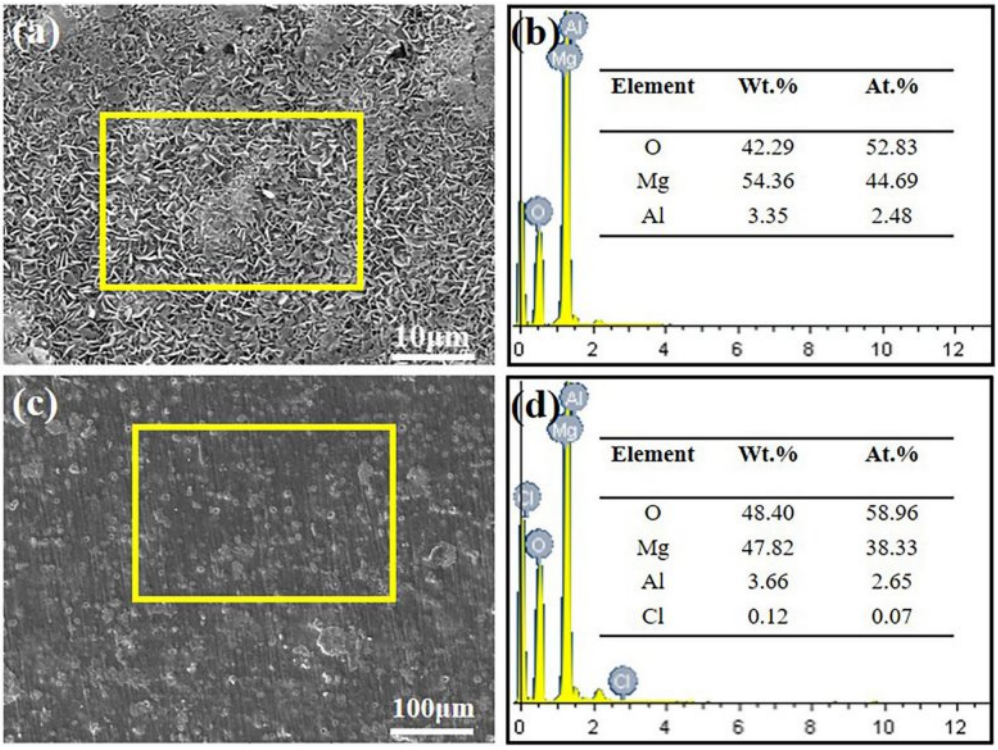

Fig. 8. EDS scanning results of SC-6 h before and after immersion.

prepared at 3 h is too thin to resist the intrusion of Cl^- in the corrosion solution, while the coating prepared at 12 h has defects in its structure despite a certain thickness. The corrosion of SC-6 h occurred only at the edge of the sample, and the coating layer of SC-6 h was relatively complete from the microscopic morphology. After the corrosion of SC-9 h samples, the existence of corrosion pits can be observed at the edges and corners of the coatings, and the corrosion resistance of the coatings prepared at 9 h is better than that of 3 h and SC-12 h, but slightly worse than that of the coatings prepared at 6 h. The structure of after immersion morphology indicates that the coating prepared for 6 h has long-term corrosion resistance, which further confirms the compactness of the coating structure. Surface scanning was performed on the SC-6 h sample surface after immersion, and the results were shown in Fig. 8. It can be seen from the surface sweep energy spectrum that chlorine appears after the coating is immersed, which proves that Cl^- enters the coating during the corrosion process.

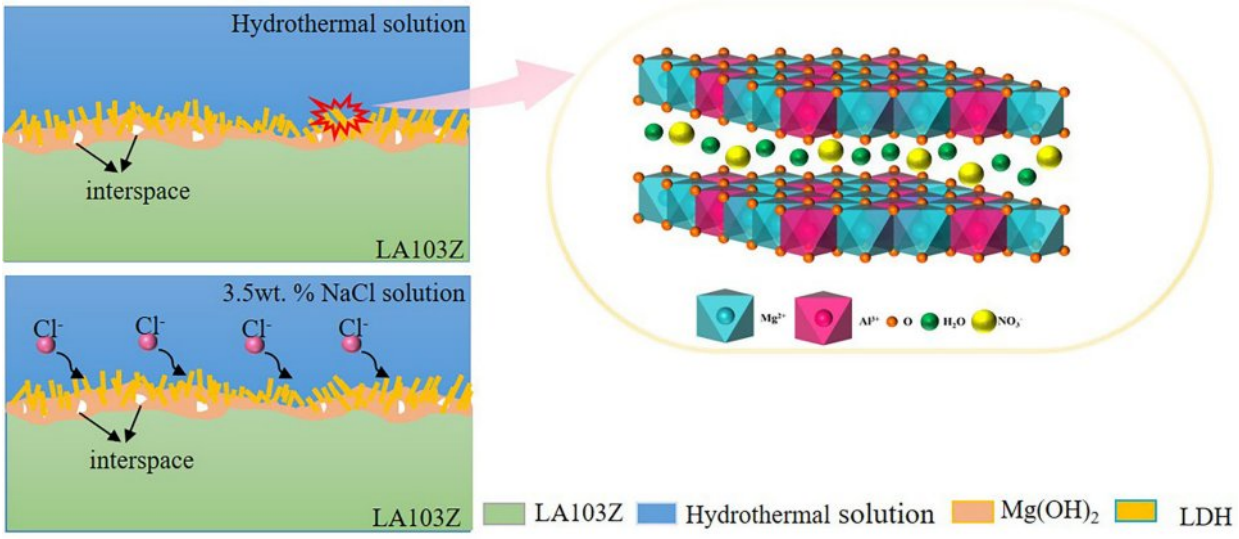

Fig. 9. Corrosion resistance mechanism of LDH.

Discussion

Growth mechanism

In this chapter, SC were successfully prepared on LA103Z substrate by in situ steam treatment. According to EDS results, XRD patterns and FT-IR patterns, it can be seen that in a closed reactor, Mg^{2+} and Al^{3+} are partially dissolved in the magnesium alloy matrix under high temperature and pressure, and Mg^{2+} and Al^{3+} are released. Water forms steam and generates heat energy under high temperature conditions, and the steam reacts with Mg^{2+} to form $Mg(OH)_2$. Under alkaline conditions, Al^{3+} exists in the form of $Al(OH)_4^-$, and some Al atoms solidly dissolved in magnesium alloys may diffuse into the crystal lattice of $Mg(OH)_2$, thus forming positively charged crystals. With the continuous heating of the reactor, $Mg(OH)_2$ reacts with $Al(OH)_4^-$ to produce LDH. In order to maintain charge balance, CO_2 in the closed environment is converted to CO_3^{2-} as the interlayer anion of the LDH. The chemical reaction of the formation process is as follows:

$$Mg + 2H_2O \rightarrow Mg(OH)_2\downarrow + H_2\uparrow \quad (2)$$

$$2Mg + O_2 \rightarrow 2MgO \quad (3)$$

$$Al^{3+} + 4OH^- \rightarrow Al(OH)_4^- \quad (4)$$

$$CO_2 + H_2O \rightarrow CO_3^{2-} + 2H^+ \quad (5)$$

$$2Al(OH)_4^- + 4Mg(OH)_2 + CO_3^{2-} + 3H_2O \rightarrow Mg_4Al_2(OH)_{12}CO_3\cdot 3H_2O + 4OH^- \quad (6)$$

According to the hydrogen evolution test and immersion morphology, Mg^{2+} and Al^{3+} do not dissolve in water during in situ steam treatment, but attach to the substrate surface and directly participate in the reaction, which greatly promotes the efficiency and densification of in-situ steam coating formation, and has a certain ability to block the invasion of corrosion solutions, but the coating thickness with the best corrosion resistance is only 2.674 μm. The restricted growth behavior of SC may be related to the following factors: Ishizaki et al. placed AMCa602 magnesium alloy in $Al(NO_3)_3$ solution with different concentrations, and prepared $Mg(OH)_2$ and Mg-Al-LDHs on its surface in situ by steam method, indicating that the Al^{3+} containing solution participated in the growth of LDH. As the concentration of $Al(NO_3)_3$ changes, the thickness of the in-situ steam coating increases, indicating that the concentration of $Al(NO_3)_3$ plays a significant role in the growth of LDH. The content of Al element produced by the dissolution of LA103Z magnesium alloy is low, which cannot provide sufficient Al source for the formation of LDH. Under high temperature conditions, the liquid phase in the closed reactor occupies most of the volume, and CO_2 is limited, which affects the formation of CO_3^{2-}, and thus affects the synthesis of LDH phase in SC. Insufficient or uneven contact between alloy and steam.

Corrosion resistance mechanism

Fig. 9 illustrates the corrosion resistance mechanism of the LDH. The corrosion resistance of SC is mainly attributed to the LDH produced on its surface. When the sample of SC is corroded, the densified LDH structure can act as a physical barrier to avoid the contact between the corrosion solution and the matrix. Therefore, the thicker the composite coating, the higher the density, and the better the physical barrier effect. The unique ion exchange and stable chemical properties of LDH are the main reasons for the effective inhibition of matrix corrosion. Nakamura et al. studied in detail the anticorrosive properties of SC in 5 wt.% NaCl solution. When the sample is immersed in 3.5 wt.% NaCl solution, the Cl^- in the solution diffuse to the solution/coating interface and are captured by LDH, which prevents the formation of soluble chloride in the coating and can play a protective role on the coating. The specific chemical reaction is as follows:

$$LDH\text{-}CO_3^{2-} + Cl^- \rightarrow CO_3^{2-} + LDH\text{-}Cl^- \quad (7)$$

At this time, the CO_3^{2-} produced diffused to the surface of the coating, competitive adsorption with Cl^- in the solution, reducing the diffusion of Cl^- to the surface of the coating, greatly reducing the damage to the coating, thus delaying the corrosion process. By comparing the morphology of the samples before and after corrosion, it can be found that LDH structure can still be observed on the surface of the sample even after a long time of corrosion, which confirms the long-term corrosion resistance of the SC.

On the other hand, the self-healing effect of LDH is also an important part of its anticorrosion process. The mechanism of this effect is dissolution/recrystallization. As the corrosion process continues, the coating begins to dissolve at the defect site, and CO_3^{2-} on the surface of the coating reacts with Mg^{2+} dissolved in the solution to form $MgCO_3$ precipitation. In an alkaline environment, $MgCO_3$ is easy to form insoluble $Mg(OH)_2$, which is covered in the corrosion damage area to form secondary protection.

$$CO_2 + H_2O \rightarrow CO_3^{2-} + 2H^+ \quad (8)$$

$$Mg \rightarrow Mg^{2+} + 2e^- \quad (9)$$

$$Mg^{2+} + CO_3^{2-} \rightarrow MgCO_3\downarrow \quad (10)$$

$$Mg^{2+} + 2OH^- \rightarrow Mg(OH)_2\downarrow \quad (11)$$

Conclusions

(1) SC were successfully prepared on the surface of LA103Z magnesium alloy by in situ steam treatment at different times (3 h, 6 h, 9 h, 12 h). The physical phase structure of SC was characterized by XRD, and the results showed that the coating was composed of

LDH, MgO and $Mg(OH)_2$ phases. The physical phase composition of SC was further analyzed by FT-IR, and the study showed that the presence of absorption peaks also confirmed that the main components of the SC were $Mg(OH)_2$ and MgO.

(2) With the extension of in situ steam treatment time, the structure of the coating increased first and then decreased. When the in situ steam treatment temperature is 110 ℃ and the time is 6 h, the prepared coating nanosheets are evenly distributed and cover the whole matrix; and the number and size were larger, the growth is perpendicular to the surface of the substrate, and the coating thickness can reach 2.674 μm.

(3) After eight days of immersion, SC-6 h showed the best corrosion resistance in the hydrogen precipitation and immersion weight loss experiments, with a small number of localized corrosion pits in the SC, but the whole was relatively flat. The amount of hydrogen precipitation per unit area was only 8.71 mL/cm^2, which was much smaller than that of the substrate (37.74 mL/cm^2).

Acknowledgements

Thanks are given to the Natural Science Basic Research Program of Shaanxi Province (Program No. 2023-JC-YB-479) and College Students' Innovation and Entrepreneurship Training Program of Shaanxi Province (No. S202210704072).

References

1. K.-A. Yasakau, A. Maltseva, S.-V. Lamaka, Di Mei, H. Orvi, P. Volovitch, M.-G.-S. Ferreiram and M.-L. Zheludkevich, Corros. Sci. 194 (2022) 109937.
2. Z.-Y. Ding, L.-Y. Cui, X.-B. Chen, R.-C. Zeng, S.-K. Guan, S.-Q. Li, F. Zhang, Y.-H. Zou, and Q.-Y. Liu, J. Alloys Compd. 764 (2018) 250-260.
3. Z.-Q. Zhang, R.-C. Zeng, C.-G. Lin, L. Wang, X.-B. Chen, and D.-C. Chen, J. Mater. Sci. Technol. 41 (2020) 43-55.
4. Y. Xia, L. Wu, W.-H. Yao, M. Hao, J. Chen, C. Zhang, T. Wu, Z.-H. Xie, J.-F. Song, B. Jiang, Y.-L. Ma, and F.-S. Pan, Trans. Nonferrous Met. Soc. China 31[6] (2021) 1612-1627.
5. H. Zhou, J.-S. Liu, D.-W. Zhou, and T. Tao, Trans. Nonferrous Met. Soc. China 30[10] (2020) 2669-2680.
6. B.-H.-A. Khaqani and N.-M. Dawood, J. Ceram. Process. Res. 25[1] (2024) 72-78.
7. C.-Y. Zhang, R.-C. Zeng, C.-L. Liu, and J.-C. G, Surf. Coat. Technol. 204[21-22] (2010) 3636-3640.
8. R.-C. Zeng, E.-H. Han, and W. Ke, Int. J. Fatigue 36[1] (2012) 40-46.
9. L.-Y. Li, L.-Y. Cui, B. Liu, R.-C. Zeng, X.-B. Chen, S.-Q. Li, Z.-L. Wang, and E.-H. Han, Appl. Surf. Sci. 465 (2019) 1066-1077.
10. L. Wu, X. Ding, Z. Zheng, Y. Ma, A. Atrens, X. Chen, Z. Xie, D. Sun, and F. Pan, Appl. Surf. Sci. 487 (2019) 558-568.
11. J. Jayaraj, K.-R. Rajesh, S.-A. Raj, A. Srinivasan, S. Ananthakumar, N.-G.-K. Dhaipule, S.-K. Kalpathy, U.-T.-S. Pillai, and U.-K. Mudali, J. Alloys Compd. 784 (2019) 1162-1174.
12. J.-H. Dou, H.-J. Yu, C.-Z. Chen, R. Lok-Wang Ma, and M. Ming-Fai Yuen, Mater. Lett. 271 (2020) 127729.
13. L.-Y. Cui, R.-C. Zeng, S.-K. Guan, W.-C. Qi, F. Zhang, S.-Q. Li, and E.-H. Han, J. Alloys Compd. 695 (2017) 2464-2476.
14. J.-Z. Lin, W.-D. Chen, Q.-Q. Tang, L.-Y. Cao, and S.-H. Su, Surf. Interfaces 22 (2021) 100805.
15. C.-A. Chen, S.-Y. Jian, C.-H. Lu, C.-Y. Lee, and M.-D. Ger, J. Mater. Res. Technol. 9[6] (2020) 13902-13913.
16. J. Jin, C. Liu, S. Fu, Y. Gao, and X. Shu, Surf. Coat. Technol. 206[2-3] (2011) 348-353.
17. Z. Liu and W. Gao, Surf. Coat. Technol. 200[11] (2007) 3553-3560.
18. J.-M. Zhang, J.-W. Wu, J.-C. Li, C.-C. Wang, B. Wang, D.-D. Lian, and M.-C. Zhang, Trans. Indian Ceram. Soc. 83[2] (2024) 126-133.
19. J.-M. Zhang, D.-D. Lian, M.-C. Zhang, A.-R. Hou, J.-C. Li, and T. Zhang, Trans. Indian Ceram. Soc. 82[2] (2024) 129-135.
20. Y.-X. Zhu, G.-L. Song, D.-J. Zheng, M. Serdechnova, C. Blawert, and M.-L. Zheludkevich, Sci. China Mater. 65[7] (2022) 1842-1852.
21. L. Ma, Y. Qiang and W. Zhao, Chem. Eng. J. 408 (2021) 127367.
22. T.-H. Nguyen, H.-N. Tran, T.-V. Nguyen, S. Vigneswaran, V.-T. Trinh, T.-D. Nguyen, T.-H. Ha Nguyen, T.-N. Mai, and H.-P. Chao, Chemosphere 295[Suppl C] (2022) 133370.
23. Y. Li, Y.-Q. Liang, X.-M. Mao, and H. Li, Chem. Eng. J. 438 (2022) 135531.
24. R.Wang, D.Wang, W.Peng, J. Zhang, J. Liu, Y. Wang, and X. Wang, Desalination 544 (2022) 116142.
25. R. Li, J.-J. Wang, B. Zhou, M.-K. Awasthi, A. Ali, Z. Zhang, L.-A. Gas-ton, A.-H. Lahori, and A. Mahar, Sci. Total Environ. 559[1] (2016) 121-129.
26. S. Zhang, Y. Chen, J. Li, Y.-F. Li, W. Song, X.-G. Li, L.-G. Yan, and H.-Q. Yu, Colloids Surf. A 641 (2022) 128584.
27. F. Peng, H. Li, D. Wang, P. Tian, Y. Tian, G. Yuan, D. Xu, and X. Liu, ACS Appl. Mater. Interfaces 8[51] (2016) 35033-35044.
28. Y. Chen, W. Li, W. Wang, Y. Zhao, and M. Chen, Ceram. Int. 48[3] (2022) 4172-4187.
29. A. Bo, S. Sarina, H. Liu, Z. Zheng, Q. Xiao, Y. Gu, G.-A. Ayoko, and H. Zhu, ACS Appl. Mater. Interfaces 8[25] (2016) 16503-16510.
30. J. Carneiro, A.-F. Caetano, A. Kuznetsova, F. Maia, A.-N. Salak, J. Te-dim, N. Scharnagl, M.-L. Zheludkevich, and M.-G.-S. Ferreira, RSC Adv. 5[50] (2015) 39916-39929.
31. J.-H. Syu, J.-Y. Uan, M.-C. Lin, and Z.-Y. Lin, Corros. Sci. 68 (2013) 238-248.
32. J.-K.-E. Tan, P. Balan, N. Birbilis, and G. Manivasagam, J. Taiwan Inst. Chem. Eng. 131[Suppl C] (2022) 104169.
33. X. Yin, P. Mu, Q. Wang, and J. Li, ACS Appl. Mater. Interfaces 12[31] (2020) 35453-35463.
34. S. Baslayici, M. Bugdayci, and M.-E. Acma, J. Ceram. Process. Res. 22[1] (2021) 98-105.
35. S.-A. Lia, Z.-Y. Yao, F.-C. Yang, G.-G. Yang, and Q.-W. Shen, J. Ceram. Process. Res. 21[4] (2020) 508-514.
36. T. Ishizaki, S. Chiba, and H. Suzuki, ECS Electrochem. Lett. 2 (2013) C15-C17.
37. T. Ishizaki, S. Chiba, K. Watanabe, and H. Suzuki, J.

Mater. Chem. A 1 (2013) 8968-8977.
38. N. Kamiyama, G. Panomsuwan, E. Yamamoto, T. Sudare, N. Saito, and T. Ishizaki, Surf. Coat. Technol. 286 (2016) 172-177.
39. J.-M. Zhang, C.-C. Wang, A.-R. Hou, J.-W. Wu, D.-D. Lian, M.-C. Zhang, and Z.-D. Yu, J. Mater. Eng. Perform. (2024) 1-10.
40. T. Ishizaki, S. Chiba, K. Watanabe, and H. Suzuki, J. Mater. Chem. A 1[31] (2013) 8968-8977.
41. C. Ke, Y. Wu, Y. Qiu, J. Duan, N. Birbilis, and X.-B. Chen, Corros. Sci. 113 (2016) 145-159.
42. K. Nakamura, Y. Shimada, T. Miyashita, A. Serizawa, and T. Ishizaki, Mater. 11[9] (2018) 1659.